

Majorana oscillations and parity crossings in semiconductor-nanowire-based transmon qubits

J. Ávila¹, E. Prada², P. San-Jose¹, R. Aguado¹

¹*Instituto de Ciencia de Materiales de Madrid (ICMM),
Consejo Superior de Investigaciones Científicas (CSIC), Sor Juana Inés de la Cruz 3,
28049 Madrid, Spain. Research Platform on Quantum Technologies (CSIC).*

²*Departamento de Física de la Materia Condensada,
Condensed Matter Physics Center (IFIMAC) and Instituto Nicolás Cabrera,
Universidad Autónoma de Madrid, E-28049 Madrid, Spain*

(Dated: October 1, 2022)

We show that the MW spectra in semiconductor-nanowire-based transmon qubits provide a strong signature of the presence of Majorana bound states in the junction. This occurs as an external magnetic field tunes the wire into the topological regime and the energy splitting of the emergent Majorana modes oscillates around zero energy owing to spatial overlap in finite-length wires. In particular, we discuss how the zero-energy fermion parity crossings arising from Majorana oscillations result in distinct spectroscopic features. In split-junction geometries, the plasma mode couples to the phase-dispersing subgap levels resulting from Majorana hybridization via a Jaynes-Cummings-like interaction. As a consequence of this interaction, higher order plasma excitations in the junction inherit Majorana properties, including the 4π effect. Our results, based on a fully microscopic description of the junction, suggest that MW spectroscopy of nanowire-based transmon qubits provides an interesting alternative to Majorana detection by transport spectroscopy.

Introduction—Superconducting islands based on Josephson junctions (JJs) shunted by a capacitor are the key element in qubits based on superconducting circuits [1–3]. Their physics is controlled by the ratio E_J/E_C between the Josephson coupling E_J and the charging energy E_C . This interplay is described by the Hamiltonian $H = 4E_C(\hat{N} - n_g)^2 + V_J(\hat{\varphi})$, where $V_J(\hat{\varphi}) = -E_J \cos \hat{\varphi}$ [4]. Here \hat{N} is the Cooper pair number, conjugate to the superconducting phase $\hat{\varphi}$, and $n_g = Q_g/2e$ is a gate-induced offset. Recent experimental efforts are pushing the standard operation limits in order to have JJs compatible with electrical gating and high magnetic fields. This compatibility is a crucial step to reach a regime relevant for microwave (MW) readout of topological qubits based on Majorana bound states (MBSs) [5–14]. Various options include semiconductors [15–21] and van der Waals heterostructures [22–24].

We here focus on a specific proposal where the JJ is based on a semiconducting nanowire (NW) that can be driven into a topological superconductor phase by means of an external Zeeman field B [25–28], see Fig. 1 (a). In this topological regime, the JJ contains MBSs which coherently interact with the superconducting island degrees of freedom. While previous theoretical studies of this problem have focused on either effective low energy toy-models [9, 10] or partial microscopic descriptions [14], our work contains a fully microscopic description, which allows to unveil new physics from the $E_J/E_C \lesssim 1$ Cooper pair box (CPB) to the $E_J \gg E_C$ transmon regimes. This includes the magnetic field dependence of NW junction parameters and the emergence of MBSs in the topological phase. Importantly, the corresponding MW spectroscopy presents signatures that fully map parity crossings in the NW spectrum owing to the oscillatory energy splitting of

overlapping Majoranas, hence providing a powerful tool for Majorana detection. In split junctions, the resulting physics generalizes that of the Jaynes-Cummings model, with multiple replicas of the plasma mode reflecting the 4π effect and Majorana oscillations.

Model—The Josephson potential is defined, on a microscopic level, as the operator $V_J(\varphi) = \frac{1}{2}\tilde{c}^\dagger H_{\text{BdG}}(\varphi)\tilde{c}$, where $\tilde{c} = (c_{i\uparrow}, c_{i\downarrow}, c_{i\uparrow}^\dagger, c_{i\downarrow}^\dagger)$ are Nambu spinors and H_{BdG} is the Bogoliubov-de Gennes (BdG) Hamiltonian

$$H_{\text{BdG}}(\varphi) = \begin{pmatrix} H_{\text{NW}} & \Delta(x, \varphi) \\ \Delta(x, \varphi)^\dagger & -H_{\text{NW}}^* \end{pmatrix}. \quad (1)$$

and where H_{NW} is the normal NW junction Hamiltonian. It consists of two segments (left/right) with normal Hamiltonians $H_{L/R}$, coupled across a short weak link of transparency $T_N \in [0, 1]$. Each segment contains all the microscopic NW details (Rashba coupling α , Zeeman field B and chemical potential μ) and is described by a single-band model $H_{L/R} = \frac{p_x^2}{2m} - \mu - \frac{\alpha}{\hbar}\sigma_y p_x + B\sigma_x$ (with $p_x = -i\hbar\partial_x$ the momentum operator and σ_i Pauli matrices in spin space). These NWs undergo a topological phase transition at $B_c \equiv \sqrt{\Delta^2 + \mu^2}$ with the appearance of MBSs at their edges, see blowup in Fig. 1 (a). $\Delta(x, \varphi) = i\sigma_y \Delta e^{\pm i\varphi/2}$ (where the \pm corresponds to $x \in L/R$, respectively) is the induced pairing term [29, 30]. While $V_J(\varphi) \sim -E_J \cos(\varphi)$ is a good approximation at $B = 0$ in the $T_N \rightarrow 0$ tunneling limit, it can strongly deviate from this form under relevant conditions (finite T_N , finite B , etc). This deviation is reflected in important qubit parameters such as the Josephson inductance and the anharmonicity [1, 17, 30].

Our goal is to derive a quantitatively precise but simple low-energy approximation for V_J , starting from its

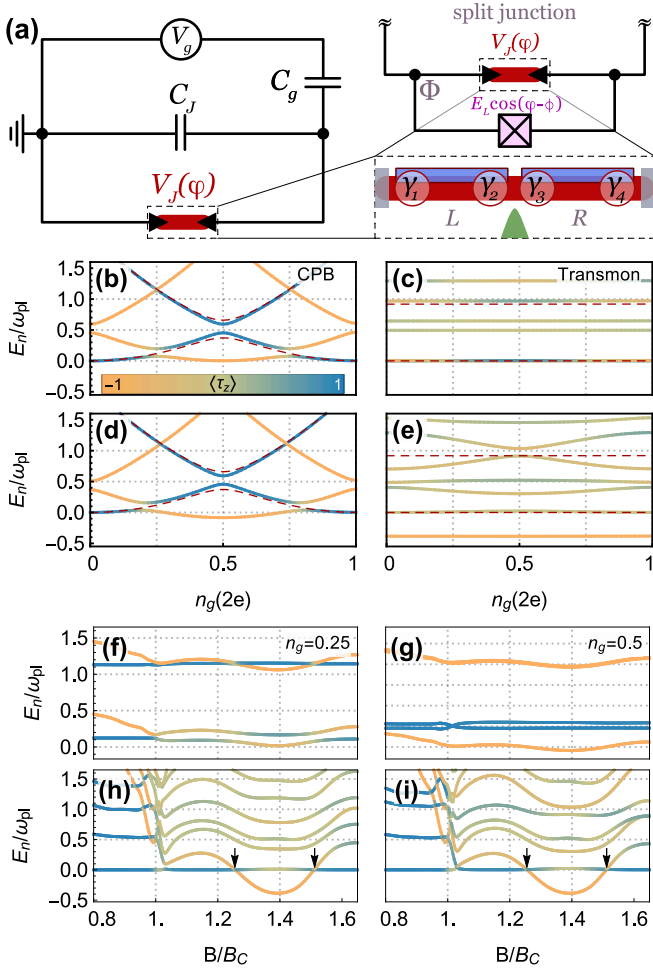


FIG. 1. **Sketch and spectrum of a NW-based superconducting qubit.** (a) Sketch of the simplified transmon/CPB qubit circuit, with a split-junction variation on the right. E_J is implicit in the Josephson potential $V_J(\varphi)$ of the nanowire junction (in red), while the combination of a shunting capacitor C_J and the gate capacitance C_g define the charging energy $E_C = e^2/2(C_J + C_g)$. γ_i represent Majorana bound states. (b-i) Blue/orange colours denote fermionic even/odd parities, while intermediate gradient signals parity mixing (see text). Panel (b): spectrum versus $n_g = V_g/(2eC_g)$ in the CPB limit ($E_J/E_C = 0.5$, $E_M/E_C \sim 0.12$) for $B = 0$ (dashed lines) and $B = 1.25B_c$ corresponding to $\delta = 0$ (coloured). Panel (c): same as (b) but in a transmon regime with $E_J/E_C = 25$, $E_M/E_C \sim 6.5$. (d) and (e) show the same CPB and transmon cases but for $\delta \neq 0$ ($B = 1.4B_c$). Panels (f,g): Magnetic field dependence for the CPB in (d), at $n_g = 0.25$ and $n_g = 0.5$, respectively. Panels (h,i): same as (f,g) but for the transmon (arrows mark parity crossings). Rest of parameters: $L_S = 2.2\mu\text{m}$, $\tau = 0.8$, $\mu = 0.5\text{meV}$, $\Delta = 0.25\text{meV}$.

microscopic form, that retains both standard Josephson events due to Cooper pair tunneling, as well as anomalous Majorana-mediated events where a single electron is transferred across the junction. While the *total* fermion parity $n \bmod 2$ is conserved (where $n = n_L + n_R$ and $n_{L,R}$ are the fermion occupations in the left/right segment

of the junction), an anomalous tunneling term changes the parity $n_{L/R} \bmod 2$ on each superconducting left/right segment. For instance, assuming even global parity, Majorana-mediated tunnelling corresponds to the process $|0\rangle \equiv |n_L = 0, n_R = 0\rangle \iff |1\rangle \equiv |n_L = 1, n_R = 1\rangle$. (In what follows, even/odd parity will always refer to the partial fermion parity $n_L \bmod 2 = n_R \bmod 2$). Physically, this suggests that to compute an effective low-energy $V_J(\varphi)$, it is convenient to distinguish two contributions, $V_J(\varphi) = V_J^{\text{bulk}}(\varphi) + H_{\text{BdG}}^{\text{sub}}$. The first one takes into account the bulk contribution of BdG levels *above* the gap, whose occupation is assumed in thermal equilibrium, $V_J^{\text{bulk}}(\varphi) = -\sum_{\epsilon_p > \Delta} \epsilon_p(\varphi)$. The second contribution corresponds to the subgap sector. By projecting H_{BdG} onto this subspace, one gets

$$H_{\text{BdG}}^{\text{sub}}(\varphi) = i\lambda_{12}\gamma_1\gamma_2 + i\lambda_{13}(\varphi)\gamma_1\gamma_3 + i\lambda_{14}(\varphi)\gamma_1\gamma_4 + i\lambda_{23}(\varphi)\gamma_2\gamma_3 + i\lambda_{24}(\varphi)\gamma_2\gamma_4 + i\lambda_{34}\gamma_3\gamma_4. \quad (2)$$

This effective form describes four subgap states (two electron-hole copies of two spin-resolved subgap states) in terms of four Majorana operators, $\gamma_{1,2} \in L$ and $\gamma_{3,4} \in R$, interacting pairwise through the λ_{ij} terms [31, 32].

Projection method—To derive the different λ_{ij} from the microscopic model itself we first calculate the Nambu spinors $\tilde{\psi}_{is}^0$ of the empty/full ($i = -, +$) lowest subgap eigenstate of each decoupled $s = L, R$ segments. These states span a fermion basis $\{c_L, c_L^\dagger, c_R, c_R^\dagger\}$ of our 4-dimensional projection space, in terms of which we can write fermion numbers as $n_L = c_L^\dagger c_L = (1 + i\gamma_1\gamma_2)/2$ and $n_R = c_R^\dagger c_R = (1 + i\gamma_3\gamma_4)/2$. We now perform a low-energy projection of the form:

$$(\mathcal{H}^{-1})_{i's', is} = \langle \tilde{\psi}_{i's'}^0 | G(\omega = 0) | \tilde{\psi}_{is}^0 \rangle, \quad (3)$$

where $G(\omega) = (\omega + i\varepsilon - H_{\text{BdG}})^{-1}$ is the resolvent of the full BdG Hamiltonian. Using this projection, Eq. (2) can be written as $H_{\text{BdG}}^{\text{sub}} = \frac{1}{2}\tilde{\psi}^{0\dagger}\mathcal{H}\tilde{\psi}^0$, which yields the different λ_{ij} . After projecting onto the parity basis $\{|p\rangle\} = \{|0\rangle, |1\rangle\}$, the final effective Hamiltonian reads

$$H = [4E_C(-i\partial_\varphi - n_g)^2 + V_J^{\text{bulk}}(\varphi)]\mathbb{1} + V_J^{\text{sub}}(\varphi). \quad (4)$$

It describes two different parity copies of a superconducting island, which are mixed through a non-diagonal term $V_J^{\text{sub}}(\varphi) = \langle p' | H_{\text{BdG}}^{\text{sub}} | p \rangle$. The parity content of the eigenstates of Eq. (4) can be calculated by a projection onto the parity axis defined by $\hat{\tau}_z \equiv |0\rangle\langle 0| - |1\rangle\langle 1|$.

We emphasize that, despite the superficial similarity with the effective low-energy model in Refs. [9, 10], Eq. (4) is derived by projecting the fully microscopic H_{BdG} . Thus, H is able to describe, in particular, the evolution of the junction from trivial to topological. This physics is captured by the three B -field-dependent microscopic energy scales [30] relevant for this problem: the Josephson coupling $E_J = \int_0^{2\pi} \frac{d\varphi}{\pi} [V_J^{\text{bulk}}(\varphi) + V_J^{\text{sub}}(\varphi)] \cos(\varphi)$, the

energy splitting between different fermionic parities $\delta = V_{J11}^{sub}(\varphi) - V_{J00}^{sub}(\varphi)|_{\varphi=0}$ and the Majorana contribution to the Josephson coupling $E_M = \int_0^{2\pi} \frac{d\varphi}{\pi} V_{J01}^{sub}(\varphi) \cos(\varphi)$.

Results—In what follows, the ratio E_J/E_C and the plasma frequency $\omega_{pl} \equiv \sqrt{8E_J E_C}/\hbar$ are defined respect to the zero-field junction, for which a microscopic calculation of I_c [29, 33, 34] gives $E_J \equiv \hbar I_c(B=0)/2e$ at fixed E_C . The fermionic parity content is represented by different colours (even/odd=blue/orange for $\langle \hat{\tau}_z \rangle = \pm 1$). In the CPB limit ($E_J/E_C = 0.5$) each even (odd) parabola in the spectrum, see Fig. 1 (b), has a minimum on $n_g = m + n_g^0$, where $m \in \mathbb{Z}$ and $n_g^0 = 0$ (0.5) (only the $m = 0, 1$ cases are shown). For $B = 0$ (dashed lines), odd parabolae are energy shifted from even ones by exactly $\delta = 2\Delta$ (outside plot range in Fig. 1 (b)), since in the state $|n_L = 1, n_R = 1\rangle$ each fermion must overcome an energy gap Δ in the left/right segment of the wire. As expected, the spectrum is $2e$ -periodic. Increasing B , the gap gets reduced until an odd ground state (GS) around $n_g = 0.5$ is possible when $\delta < E_C$. In the $\delta \rightarrow 0$ limit, both parity sectors have minima at zero energy and the periodicity becomes e [35, 36], Fig. 1 (b). Furthermore, both sectors are coherently mixed around $n_g = 0.25$ and $n_g = 0.75$ (lighter regions) due to MBSs [9, 10, 14]. In the transmon limit, Fig. 1 (c), the presence of MBSs manifests as splitting of the transmon lines which show strong parity mixing for all n_g .

The above phenomenology depends on the ratio ξ_M/L_S , with ξ_M the Majorana coherence length (which depends on B [37]) and L_S the NW length, which in turn governs the energy splitting δ [38]. Figures 1 (d,e) illustrate this effect where we plot the same spectra but at a different B corresponding to $\delta \neq 0$. Interestingly, the spectrum is now $2e$ -periodic for both the CPB and transmon limits. In this latter case, Fig. 1 (e), the overall n_g dependence differs considerably from a standard transmon [compare with Fig. 1 (c)]. Note also that the (odd) parity of the GS is well defined for all n_g .

We now focus on the magnetic field evolution of the island spectrum. In the CPB regime, this evolution strongly depends on gate (owing to the large charge dispersion). Since parity mixing occurs near $n_g = 0.25$, the B -field dependence at this gate considerably differs from the one at $n_g = 0.5$, where parity mixing is negligible, compare Figs. 1 (f) and (g). In the transmon limit, the spectrum mimics Majorana oscillations and shows alternating GS parities (change of colour from blue to orange and back) after each parity crossing [see arrows in Fig. 1 (h,i)]. This behaviour occurs for all n_g . These parity transitions in the GS have important consequences for MW spectroscopy, as we shall discuss next. Before that, we just mention that these switches of GS parity are possible since, for the single band case considered here, E_M is non-negligible as compared to E_J [29, 30, 33, 34, 39]. Consequently, in a transmon regime with $E_J/E_C \gg 1$, the ratio E_M/E_C is not small. Considering typical crit-

ical current values $I_c \sim 0.2I_0$, with $I_0 = e\Delta/\hbar$ the maximum supercurrent of a single open channel, this gives $E_J \sim 0.1\Delta \sim 25\mu\text{eV} \sim 6\text{GHz}$, assuming an induced gap of the order $\Delta \sim 250\mu\text{eV}$. A conservative estimate $E_M \sim 0.5E_J \sim 0.05\Delta$ yields $E_M \sim 12.5\mu\text{eV} \sim 3\text{GHz}$, which compared to typical charging energies in the transmon regime $E_C \sim 300\text{MHz}$ [15–17] indeed gives $E_M/E_C \sim 10$. This relevant regime has hitherto remained unexplored, even at the level of the effective models in Refs. [9, 10, 14] which focus on the opposite $E_M/E_C \ll 1$ regime. This would require much larger charging energies (which is detrimental for the transmon since they induce charge dispersion) or Majorana couplings well below the above estimation. The latter can be, however, somewhat difficult to reach in a few-channel topological wire: while more than one channel can contribute to E_J [17, 40, 41], the value of E_M is in turn governed by the topological minigap from a single-channel Majorana Josephson effect. In this few channel situation, the above estimation of E_M/E_C would be reduced by a factor $\sim 1/N$, with N the number of trivial channels contributing to E_J [30].

MW spectroscopy—By considering a capacitive coupling to a small periodic perturbation in the gate voltage, the resulting linear-response MW absorption spectrum reads $S_N(\omega) = \sum_n |\langle n | \hat{N} | 0 \rangle|^2 \delta(\omega - \omega_{n0})$, where Ψ_n are the eigenstates of Eq. (4) and $\omega_{n0} = (E_n - E_0)/\hbar$. In what follows we focus on the transmon limit with $E_M/E_C \gtrsim 1$, realized by a single band nanowire in the topological regime. A full discussion about other relevant parameter regimes, including the CPB and the transmon regime with $E_M/E_C \ll 1$, can be found in Ref. [30]. In Fig. 2 (a) we plot the magnetic field dependence of the MW spectrum in the transmon regime for $n_g = 0.5$. Majorana oscillations and parity switches in Fig. 1 (i) are found to result in abrupt spectroscopic changes at B fields where Majorana oscillations have nodes. They include spectral *holes* in the first transition (corresponding to a low-energy transition owing to Majorana-mediated parity mixing) accompanied by higher transition lines suddenly disappearing/appearing. The spectral holes can be understood as exact cancellations of spectral weight owing to parity degeneracy at crossings. This is illustrated in Fig. 2 (b) where we plot the transition frequencies weighted by their respective matrix element (represented as the width of the line). Together with the absence of spectral weight of the ω_{01} transition at crossings, there is a complete spectral weight transfer between higher energy transitions, where one thick line becomes thin or viceversa (see arrows). Figs. 2 (c-e) show the n_g dependence for three fixed B fields [coloured bars in (a)] across a parity crossing. Interestingly, all the spectroscopic features before and after the crossing [(c) and (e), respectively] are shifted exactly by one e unit, which reflects the change of parity of the GS. See also the transitions weighted by their matrix elements in Figs. 2 (f-h). This results in distinct spectroscopic features like spectral

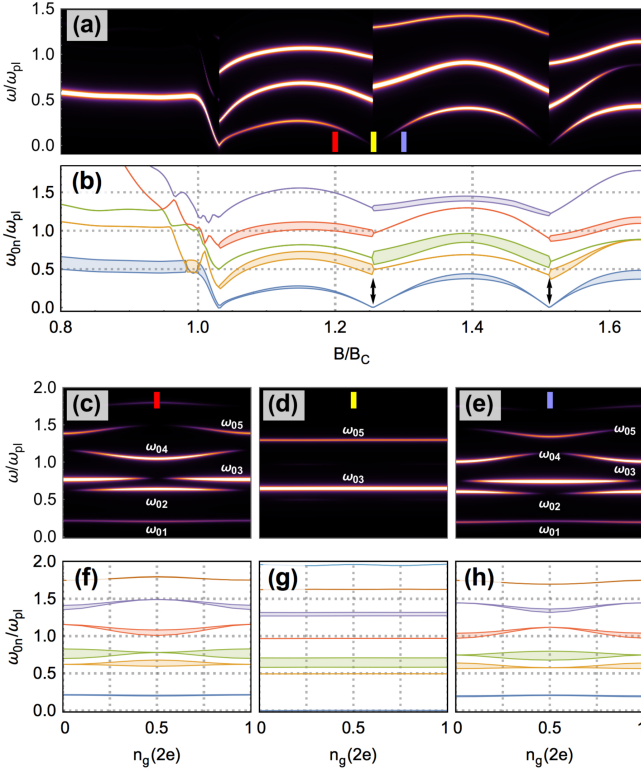


FIG. 2. **MW spectroscopy of a NW-based transmon.** Panel (a): contour plot of MW absorption spectrum $S_N(\omega)$ versus ω and B/B_c at $n_g = 0.5$. Bright lines signal allowed transitions in the MW response. Spectral holes in the $n = 1$ transition line and abrupt jumps in the $n > 1$ ones, where lines suddenly disappear/appear, coincide with parity crossings in the GS owing to Majorana oscillations. (b): Transition frequencies and spectral weights (shadowed widths). At minima of the oscillations (arrows), the spectral weight of different transitions gets exchanged. Panels (c-h): n_g dependence. Same parameters as the transmon in Fig. 1.

holes that shift from half-integer to integer values of n_g and viceversa, and changes of curvatures of the involved transitions. Right at the $\delta = 0$ parity crossing, (d,g), we recover a standard transmon spectrum. Such unique behaviour of transmon spectra across a Majorana oscillation should provide a strong signature of the presence of MBSs and their associated parity crossings.

Split junction geometry—We next consider a split-junction where a standard ancillary JJ in parallel with the NW JJ forms a loop which is threaded by an external flux Φ , see Fig. 1 (a) right panel. The Josephson potential is then split into two terms $-E_L \cos(\hat{\varphi}) + V_J(\phi - \hat{\varphi})$, where $\phi \equiv 2\pi\Phi/\Phi_0$ with $\Phi_0 = h/2e$ the flux quantum. When $E_L \gg E_C$, fluctuations of $\hat{\varphi}$ are small and centered around zero, while the external phase mostly drops over the NW JJ. In this limit, the dependence on n_g is irrelevant and one is left with an effective LC harmonic oscillator $H_b \sim E_C \hat{N}^2 + \frac{E_L}{2} \hat{\varphi}^2 = \hbar\omega_{pl}(b^\dagger b + \frac{1}{2})$, with plasma frequency $\omega_{pl} = \sqrt{8E_L E_C}/\hbar$, which interacts

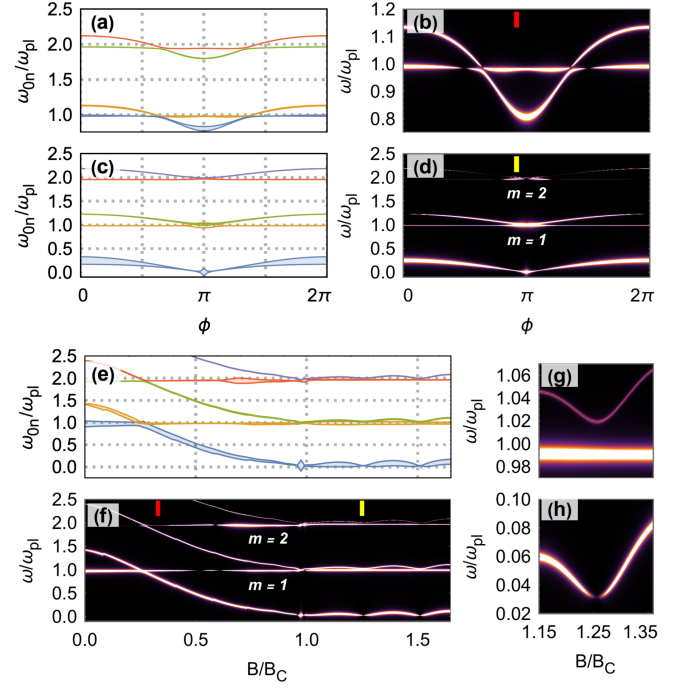


FIG. 3. **MW spectroscopy in a split-junction geometry** with $E_L/E_J = 60$. NW parameters as in Fig. 2. Panel (a): Phase dispersion of the transition frequencies and their spectral weights (widths of the lines) in the trivial regime $B = 0.33B_c$. (b) Blowup of the corresponding MW spectrum showing the avoided crossing between the plasma mode and the Andreev level in the NW junction. (c) and (d): Same in the topological regime $B = 1.25B_c$ showing plasma replicas of the underlying 4π effect in the NW junction. (e) and (f): Magnetic field dependence near $\phi = \pi$. Panels (g) and (h) show a blowup near the first minimum at $B \approx 1.25B_c$.

with the phase-dispersing levels of the NW JJ through an inductive term $H_I = -\frac{\Phi_0}{2\pi} \hat{\varphi} \hat{I}$, with $\hat{\varphi} = (\frac{E_C}{8E_L})^{1/4}(b^\dagger + b)$ [14, 42]. In practice, we calculate the current operator in the eigenbasis that diagonalizes the NW JJ effective Hamiltonian, $\hat{I} = \frac{\partial V_J(\varphi)}{\partial \varphi} = \frac{\partial}{\partial \varphi}(\sum_k E_k |k\rangle \langle k|)$. In this configuration, the visibility of the allowed MW transitions is just given by the matrix elements $\langle n | \hat{I} | 0 \rangle$. The above model generalizes the Jaynes-Cummings model that results from considering only one Andreev level in the junction [43–46]. Indeed, the topologically trivial $B < B_c$ regime captures this Jaynes-Cummings physics where an Andreev level strongly dispersing with phase $E_A(\phi)$ anticrosses with the plasma mode [Figs. 3 (a,b)], in good agreement with previous experiments [45–47]. When $B > B_c$, the levels show a characteristic phase dispersion with a zero-energy crossing at $\phi = \pi$ (the so-called 4π effect), see Figs. 3 (c,d). Apart from the fundamental transition, the MW response shows higher order processes where m plasma modes are excited, which results in transitions occurring at $m\omega_{pl}$ and $E_A(\phi) + m\omega_{pl}$ [47], see Figs. 3 (c,d). Interestingly, the residual splittings at $\phi = \pi$ owing to Majorana overlaps [31, 32] are

imprinted on each of these replicas, which, near $\phi = \pi$, mimic the oscillatory Majorana behavior as a function of B [Figs. 3 (e,f)]. As before, minima of the Majorana oscillations result in spectral holes.

In summary, our results demonstrate that MW spectroscopy of NW-based transmon qubits is a powerful tool to detect the presence of MBSs in the JJ junction, including Majorana oscillations, parity crossings and the 4π effect. This provides a detection scheme alternative to tunneling spectroscopy [48]. Our projection method can be readily extended to other relevant NW regimes not discussed here, like multiband NWs [34] or other qubit regimes [30]. Other geometries currently under intensive experimental study, including junctions with quantum dots [49, 50] and superconducting islands in the fluxonium regime [51], should be the subject of future studies.

We thank Bernard van Heck for his input. Research supported by the Spanish Ministry of Science and Innovation through Grants PGC2018-097018-B-I00, FIS2016-80434-P (AEI/FEDER, EU), BES-2016-078122 (FPI programme), and RYC-2011-09345 (Ramón y Cajal programme). The EU Horizon 2020 research and innovation programme (FETOPEN Grant Agreement No. 828948) and the CSIC Research Platform on Quantum Technologies PTI-001 are also acknowledged.

-
- [1] A. Blais, R.-S. Huang, A. Wallraff, S. M. Girvin, and R. J. Schoelkopf, *Phys. Rev. A* **69**, 062320 (2004).
 - [2] M. H. Devoret and R. J. Schoelkopf, *Science* **339**, 1169 (2013).
 - [3] G. Wendin, *Reports on Progress in Physics* **80**, 106001 (2017).
 - [4] V. Bouchiat, D. Vion, P. Joyez, D. Esteve, and M. H. Devoret, *Physica Scripta* **T76**, 165 (1998).
 - [5] F. Hassler, A. R. Akhmerov, and C. W. J. Beenakker, *New Journal of Physics* **13**, 095004 (2011).
 - [6] C. Müller, J. Bourassa, and A. Blais, *Phys. Rev. B* **88**, 235401 (2013).
 - [7] D. Pekker, C.-Y. Hou, V. E. Manucharyan, and E. Demler, *Phys. Rev. Lett.* **111**, 107007 (2013).
 - [8] P. Virtanen and P. Recher, *Phys. Rev. B* **88**, 144507 (2013).
 - [9] E. Ginossar and E. Grosfeld, *Nature communications* **5**, 4772 (2014).
 - [10] K. Yavilberg, E. Ginossar, and E. Grosfeld, *Phys. Rev. B* **92**, 075143 (2015).
 - [11] O. Dmytruk, M. Trif, and P. Simon, *Phys. Rev. B* **92**, 245432 (2015).
 - [12] M. C. Dartiaillh, T. Kontos, B. Douçot, and A. Cottet, *Phys. Rev. Lett.* **118**, 126803 (2017).
 - [13] M. Trif, O. Dmytruk, H. Bouchiat, R. Aguado, and P. Simon, *Phys. Rev. B* **97**, 041415 (2018).
 - [14] A. Keselman, C. Murthy, B. van Heck, and B. Bauer, *SciPost Phys.* **7**, 50 (2019).
 - [15] T. W. Larsen, K. D. Petersson, F. Kuemmeth, T. S. Jespersen, P. Krogstrup, J. Nygård, and C. M. Marcus, *Phys. Rev. Lett.* **115**, 127001 (2015).
 - [16] G. de Lange, B. van Heck, A. Bruno, D. J. van Woerkom, A. Geresdi, S. R. Plissard, E. P. A. M. Bakkers, A. R. Akhmerov, and L. DiCarlo, *Phys. Rev. Lett.* **115**, 127002 (2015).
 - [17] A. Kringhøj, L. Casparis, M. Hell, T. W. Larsen, F. Kuemmeth, M. Leijnse, K. Flensberg, P. Krogstrup, J. Nygård, K. D. Petersson, and C. M. Marcus, *Phys. Rev. B* **97**, 060508 (2018).
 - [18] L. Casparis, T. W. Larsen, M. S. Olsen, F. Kuemmeth, P. Krogstrup, J. Nygård, K. D. Petersson, and C. M. Marcus, *Phys. Rev. Lett.* **116**, 150505 (2016).
 - [19] F. Luthi, T. Stavenga, O. W. Enzing, A. Bruno, C. Dickel, N. K. Langford, M. A. Rol, T. S. Jespersen, J. Nygård, P. Krogstrup, and L. DiCarlo, *Phys. Rev. Lett.* **120**, 100502 (2018).
 - [20] L. Casparis, N. J. Pearson, A. Kringhøj, T. W. Larsen, F. Kuemmeth, J. Nygård, P. Krogstrup, K. D. Petersson, and C. M. Marcus, *Phys. Rev. B* **99**, 085434 (2019).
 - [21] L. Casparis, M. R. Connolly, M. Kjaergaard, N. J. Pearson, A. Kringhøj, T. W. Larsen, F. Kuemmeth, T. Wang, C. Thomas, S. Gronin, G. C. Gardner, M. J. Manfra, C. M. Marcus, and K. D. Petersson, *Nature Nanotechnology* **13**, 915 (2018).
 - [22] J. G. Kroll, W. Uilhoorn, K. L. van der Enden, D. de Jong, K. Watanabe, T. Taniguchi, S. Goswami, M. C. Cassidy, and L. P. Kouwenhoven, *Nature Communications* **9**, 4615 (2018).
 - [23] F. E. Schmidt, M. D. Jenkins, K. Watanabe, T. Taniguchi, and G. A. Steele, *Nature Communications* **9**, 4069 (2018).
 - [24] J. I.-J. Wang, D. Rodan-Legrain, L. Bretheau, D. L. Campbell, B. Kannan, D. Kim, M. Kjaergaard, P. Krantz, G. O. Samach, F. Yan, J. L. Yoder, K. Watanabe, T. Taniguchi, T. P. Orlando, S. Gustavsson, P. Jarillo-Herrero, and W. D. Oliver, *Nature Nanotechnology* **14**, 120 (2019).
 - [25] R. M. Lutchyn, J. D. Sau, and S. Das Sarma, *Phys. Rev. Lett.* **105**, 077001 (2010).
 - [26] Y. Oreg, G. Refael, and F. von Oppen, *Phys. Rev. Lett.* **105**, 177002 (2010).
 - [27] R. Aguado, *Riv. Nuovo Cimento* **40**, 523 (2017).
 - [28] R. M. Lutchyn, E. P. A. M. Bakkers, L. P. Kouwenhoven, P. Krogstrup, C. M. Marcus, and Y. Oreg, *Nature Reviews Materials* **3**, 52 (2018).
 - [29] J. Cayao, P. San-Jose, A. M. Black-Schaffer, R. Aguado, and E. Prada, *Phys. Rev. B* **96**, 205425 (2017).
 - [30] J. Avila, E. Prada, P. San-Jose, and R. Aguado, (2020), submitted.
 - [31] P. San-Jose, E. Prada, and R. Aguado, *Phys. Rev. Lett.* **108**, 257001 (2012).
 - [32] D. I. Pikulin and Y. V. Nazarov, *Phys. Rev. B* **86**, 140504 (2012).
 - [33] P. San-Jose, J. Cayao, E. Prada, and R. Aguado, *New J. Phys.* **15**, 075019 (2013).
 - [34] P. San-Jose, E. Prada, and R. Aguado, *Phys. Rev. Lett.* **112**, 137001 (2014).
 - [35] S. M. Albrecht, A. P. Higginbotham, M. Madsen, F. Kuemmeth, T. S. Jespersen, J. Nygård, P. Krogstrup, and C. M. Marcus, *Nature* **531**, 206 (2016).
 - [36] J. Shen, S. Heedt, F. Borsoi, B. van Heck, S. Gazibegovic, R. L. M. Op het Veld, D. Car, J. A. Logan, M. Pendharkar, S. J. J. Ramakers, G. Wang, D. Xu, D. Bouman, A. Geresdi, C. J. Palmstrøm, E. P. A. M. Bakkers, and L. P. Kouwenhoven, *Nature Communications* **9**, 4801 (2018).

- (2018).
- [37] R. V. Mishmash, D. Aasen, A. P. Higginbotham, and J. Alicea, *Phys. Rev. B* **93**, 245404 (2016).
 - [38] This claim is only true for spatially-homogeneous wires since a smooth $\mu(x)$ can lead to $\delta \rightarrow 0$ irrespective of the ratio ξ_M/L_S , see Ref. [48] and references therein.
 - [39] J. Tiira, E. Strambini, M. Amado, S. Roddaro, P. San-Jose, R. Aguado, F. S. Bergeret, D. Ercolani, L. Sorba, and F. Giazotto, *Nat. Commun.* **8**, 14984 (2017).
 - [40] M. F. Goffman, C. Urbina, H. Pothier, J. Nygård, C. M. Marcus, and P. Krogstrup, *New Journal of Physics* **19**, 092002 (2017).
 - [41] L. Tosi, C. Metzger, M. F. Goffman, C. Urbina, H. Pothier, S. Park, A. L. Yeyati, J. Nygård, and P. Krogstrup, *Phys. Rev. X* **9**, 011010 (2019).
 - [42] M. A. Despósito and A. Levy Yeyati, *Phys. Rev. B* **64**, 140511 (2001).
 - [43] G. Romero, I. Lizuain, V. S. Shumeiko, E. Solano, and F. S. Bergeret, *Phys. Rev. B* **85**, 180506 (2012).
 - [44] L. Bretheau, Ç. Ö. Girit, M. Houzet, H. Pothier, D. Esteve, and C. Urbina, *Phys. Rev. B* **90**, 134506 (2014).
 - [45] D. J. van Woerkom, A. Proutski, B. van Heck, D. Bouman, J. I. Väyrynen, L. I. Glazman, P. Krogstrup, J. Nygård, L. P. Kouwenhoven, and A. Geresdi, *Nature Physics* **13**, 876 (2017).
 - [46] M. Hays, G. de Lange, K. Serniak, D. J. van Woerkom, D. Bouman, P. Krogstrup, J. Nygård, A. Geresdi, and M. H. Devoret, *Phys. Rev. Lett.* **121**, 047001 (2018).
 - [47] L. Bretheau, C. O. Girit, H. Pothier, D. Esteve, and C. Urbina, *Nature* **499**, 312 (2013).
 - [48] E. Prada, P. San-Jose, M. W. A. de Moor, A. Geresdi, E. J. H. Lee, J. Klinovaja, D. Loss, J. Nygård, R. Aguado, and L. P. Kouwenhoven, (2019), arXiv:1911.04512.
 - [49] A. Bargerbos, W. Uilhoorn, C.-K. Yang, P. Krogstrup, L. P. Kouwenhoven, G. de Lange, B. van Heck, and A. Kou, (2019), arXiv:1911.10010.
 - [50] A. Kringhøj, B. van Heck, T. W. Larsen, O. Erlandsson, D. Sabonis, P. Krogstrup, L. Casparis, K. D. Petersson, and C. M. Marcus, (2019), arXiv:1911.10011.
 - [51] M. Pita-Vidal, A. Bargerbos, C.-K. Yang, D. J. van Woerkom, W. Pfaff, N. Haider, P. Krogstrup, L. P. Kouwenhoven, G. de Lange, and A. Kou, (2019), arXiv:1910.07978.